Science
AAAS

Direct Observations of Atmospheric Aerosol Nucleation
Markku Kulmala *et al.*
Science **339**, 943 (2013);
DOI: 10.1126/science.1227385

Science (print ISSN 0036-8075; online ISSN 1095-9203) is published weekly, except the last week in December, by the American Association for the Advancement of Science, 1200 New York Avenue NW, Washington, DC 20005.

structured influence of groundwater on land hydrology and ecosystems and highlight the need for larger efforts to improve observing and modeling large-scale groundwater processes in the context of earth system dynamics.

References and Notes

1. T. C. Winter, J. W. Harvey, O. L. Franke, W. A. Alley, "Ground water and surface water: A single resource" (USGS Circular 1139, U.S. Government Printing Office, Denver, CO, 1998).
2. G. Miguez-Macho, Y. Fan, *J. Geophys. Res.* **117**, (D15), D15113 (2012a).
3. Y. Fan, G. Miguez-Macho, *Clim. Dyn.* **37**, 253 (2011).
4. G. Miguez-Macho, Y. Fan, *J. Geophys. Res.* **117**, (D15), D15114 (2012b).
5. D. C. Martre, D. F. Scott, C. Colvin, *Water S.A.* **25**, 137 (1999).
6. F. Orellana, P. Verma, S. P. Loheide II, E. Daly, *Rev. Geophys.* **50**, RG3003 (2012).
7. D. R. Rossatto, L. de Carvalho Ramos Silva, R. Villalobos-Vega, L. S. L. Sternberg, A. C. Franco, *Environ. Exp. Bot.* **77**, 259 (2012).
8. P. Döll, K. Fiedler, *Hydrol. Earth Syst. Sci.* **12**, 863 (2008).
9. M. Giordano, *Annu. Rev. Environ. Resour.* **34**, 153 (2009).
10. T. L. Gleeson *et al.*, *Geophys. Res. Lett.* **38**, L02401 (2011).
11. T. R. Green *et al.*, *J. Hydrol.* **405**, 532 (2011).
12. A. M. MacDonald, H. C. Bonsor, B. E. O. Docharaigh, R. G. Taylor, *Environ. Res. Lett.* **7**, 024009 (2012).
13. R. G. Taylor *et al.*, *Nat. Clim. Change* **3**, nclimate1744 (2012).
14. Materials and methods are available as supplementary material on *Science* Online.
15. H. F. Faure, R. C. Walter, D. R. Grant, *Global Planet. Change* **33**, 47 (2002).
16. B. A. Hawkins *et al.*, *Ecology* **84**, 3105 (2003).
17. H. Kreft, W. Jetz, *Proc. Natl. Acad. Sci. U.S.A.* **104**, 5925 (2007).
18. E. G. Jobbágy, M. D. Nosetto, P. E. Villagra, R. B. Jackson, *Ecol. Appl.* **21**, 678 (2011).
19. B. M. J. Engelbrecht *et al.*, *Nature* **447**, 80 (2007).
20. C. E. T. Paine, K. E. Harms, J. Ramos, *J. Trop. Ecol.* **25**, 171 (2009).
21. K. A. Dwire, J. B. Kauffman, J. E. Baham, *Wetlands* **26**, 131 (2006).
22. A. J. Elmore, J. F. Mustard, S. J. Manning, *Ecol. Appl.* **13**, 443 (2003).
23. J. Grogan, J. Galvao, *Acta Amazon.* **36**, 483 (2006).
24. F. M. R. Hughes, *J. Biogeogr.* **15**, 127 (1988).
25. S. Jirka *et al.*, *J. Veg. Sci.* **18**, 183 (2007).
26. R. Pélissier, S. Dray, D. Sabatier, *Plant Ecol.* **162**, 143 (2002).
27. M. A. Sobrado, *J. Trop. Ecol.* **26**, 215 (2010).
28. J. C. Stromberg, R. Tiller, B. Richter, *Ecol. Appl.* **6**, 113 (1996).
29. A. A. Bobrov, D. J. Charman, B. G. Warner, *Protist* **150**, 125 (1999).
30. S. K. Arndt, A. Kahmen, C. Arampatsis, M. Popp, M. Adams, *Oecologia* **141**, 385 (2004).
31. M. R. Bakker, L. Augusto, D. L. Achat, *Plant Soil* **286**, 37 (2006).
32. J. L. Carter, D. A. White, *Tree Physiol.* **29**, 1407 (2009).
33. H. S. Mishra, T. R. Rathore, V. S. Tomar, *Irrig. Sci.* **18**, 117 (1999).
34. J. Stave, G. Oba, A. B. Eriksen, I. Nordal, N. C. Stenseth, *For. Ecol. Manage.* **212**, 367 (2005).

Acknowledgments: We thank many individuals for making and providing observations (full acknowledgement is in the supplementary materials) and P. Döll for providing recharge estimates. Funding comes from U.S. National Science Foundation (NSF-AGS-1045110 and NSF-OCE-10409088), U.S. Environmental Protection Agency (EPA-STAR-RD834190), European Commission FP7 (GLOWASIS), and a Rutgers University Board of Trustees grant (651201). Computation used the Extreme Science and Engineering Discovery Environment (XSEDE) supported by U.S. National Science Foundation (NSF-OCI-1053575) and the Climate Simulation Laboratory at NCAR's Computational and Information Systems Laboratory, sponsored by the National Science Foundation and other agencies. Observations, code, and model results are accessible at https://glowasis.deltares.nl/thredds/catalog/opendap/opendap/Equilibrium_Water_Table/catalog.html.

Supplementary Materials

www.sciencemag.org/cgi/content/full/339/6122/940/DC1
Supplementary Text
Figs. S1 to S17
Tables S1 to S3
References (*35*–*228*)
Databases S1 to S3

10.1126/science.1229881

Direct Observations of Atmospheric Aerosol Nucleation

Markku Kulmala,[1]* Jenni Kontkanen,[1] Heikki Junninen,[1] Katrianne Lehtipalo,[1] Hanna E. Manninen,[1] Tuomo Nieminen,[1,14] Tuukka Petäjä,[1] Mikko Sipilä,[1] Siegfried Schobesberger,[1] Pekka Rantala,[1] Alessandro Franchin,[1] Tuija Jokinen,[1] Emma Järvinen,[1] Mikko Äijälä,[1] Juha Kangasluoma,[1] Jani Hakala,[1] Pasi P. Aalto,[1] Pauli Paasonen,[1] Jyri Mikkilä,[2] Joonas Vanhanen,[2] Juho Aalto,[3] Hannele Hakola,[4] Ulla Makkonen,[4] Taina Ruuskanen,[1] Roy L. Mauldin III,[1,5] Jonathan Duplissy,[1] Hanna Vehkamäki,[1] Jaana Bäck,[6] Aki Kortelainen,[7] Ilona Riipinen,[8] Theo Kurtén,[1,9] Murray V. Johnston,[10] James N. Smith,[7,11] Mikael Ehn,[1,12] Thomas F. Mentel,[12] Kari E. J. Lehtinen,[4,7] Ari Laaksonen,[4,7] Veli-Matti Kerminen,[1] Douglas R. Worsnop[1,4,7,13]

Atmospheric nucleation is the dominant source of aerosol particles in the global atmosphere and an important player in aerosol climatic effects. The key steps of this process occur in the sub–2-nanometer (nm) size range, in which direct size-segregated observations have not been possible until very recently. Here, we present detailed observations of atmospheric nanoparticles and clusters down to 1-nm mobility diameter. We identified three separate size regimes below 2-nm diameter that build up a physically, chemically, and dynamically consistent framework on atmospheric nucleation—more specifically, aerosol formation via neutral pathways. Our findings emphasize the important role of organic compounds in atmospheric aerosol formation, subsequent aerosol growth, radiative forcing and associated feedbacks between biogenic emissions, clouds, and climate.

Atmospheric aerosol formation [that is, the formation of molecular clusters and their growth to larger sizes (*1*, *2*)] has an important effect on aerosol particle number concentrations (*3*, *4*) and on climate through indirect radiative effects (*5*, *6*). To understand the initial steps of atmospheric aerosol formation, one must have detailed knowledge of the concentrations of neutral and charged clusters, their chemical composition, and gaseous compounds participating in their formation and growth. However, size-segregated measurements of sub–2-nm clusters are extremely rare, and until now, no one has taken comprehensive and simultaneous field measurements of charged and neutral clusters and their precursors (supplementary materials, section 3).

Recent technical developments make it possible to measure the concentrations and size distributions of ions, molecular clusters, and nanoparticles in the 1- to 2-nm mobility diameter range and to simultaneously obtain information about the chemical composition of these entities and their interactions with trace gases. Here, we present a comprehensive analysis of such measurements, conducted between 14 March and 16 May 2011, at the SMEAR II station (*7*) in Hyytiälä, southern Finland. We measured the total nanoparticle and ion concentrations, along with the concentrations of gaseous compounds, including sulfuric acid, volatile organic compounds, ammonia, amines, ozone, sulfur dioxide, and nitrogen oxides. The instruments we used to take our measurements are described in greater detail in the supplementary materials (sections 1.3.1 to 1.3.7).

We categorized each day of the measurement campaign as a "nucleation event day," a "non-event day," or an "undefined day" (table S7) (*8*). We determined the concentrations of nanoparticles and ions separately for six size classes between 0.9 and 2.1 nm (supplementary materials, section 1.2). For each size class, we calculated the concentration of nanoparticles originating from neutral formation pathways, N_n, from the relation $N_{tot} = N_{ions} + N_{rec} + N_n$, where N_{tot} is the total measured nanoparticle concentration in that size class, N_{ions} is the corresponding ion concentration, and N_{rec} is the estimated concentration of neutral particles originating from the recombination of

[1]Department of Physics, University of Helsinki, Finland. [2]Airmodus Oy, Helsinki, Finland. [3]SMEAR Station II, Hyytiälä, Finland. [4]Finnish Meteorological Institute, Finland. [5]University of Colorado at Boulder, Boulder, CO, USA. [6]Department of Forest Sciences, University of Helsinki, Finland. [7]University of Eastern Finland, Kuopio, Finland. [8]University of Stockholm, Stockholm, Sweden. [9]Department of Chemistry, University of Helsinki, Finland. [10]University of Delaware, Newark, DE, USA. [11]National Center for Atmospheric Research, Boulder, CO, USA. [12]Forschungszentrum Juelich, IEK-8, 52425 Juelich, Germany. [13]Aerodyne Research, Billerica, MA, USA. [14]Helsinki Institute of Physics, Helsinki, Finland.

*To whom correspondence should be addressed. E-mail: markku.kulmala@helsinki.fi

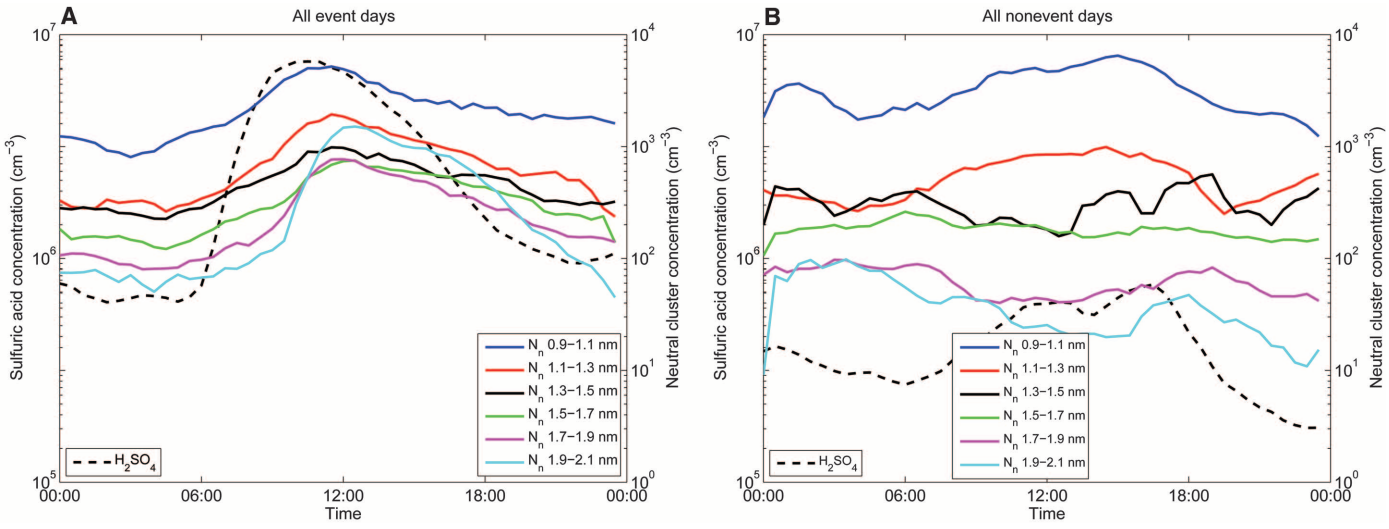

Fig. 1. Diurnal variations of the sulfuric acid concentration (left *y* axis) and the concentrations of neutral clusters in different size classes (right *y* axis) during median event days (**A**) and median nonevent days (**B**).

oppositely charged ions ending up in that size class (supplementary materials, section 1.2).

Excluding a few intermittent periods during the night, N_n exceeded N_{ions} and N_{rec} in all of the sub–2-nm size classes (fig. S9). The dominance of neutral nanoparticles over ions was particularly clear during the periods of active aerosol formation, characterized by the measurable formation of 3-nm particles and their further growth to larger sizes (see fig. S8A). Ions showed a clear concentration maximum below 1.5 nm and a steep concentration decrease above this size under all conditions (fig. S9A). Such a maximum corresponds to the size of stable ion clusters in the ion-induced nucleation theory. Overall, our observations indicate that the dynamics of sub–2-nm clusters were dominated by neutral pathways, with little influence due to the presence of ions. This finding is in line with the latest analysis of earlier field measurements conducted in various continental boundary-layer environments (*9*). Hereafter, we will focus our attention on the properties of neutral nanoparticles and call them "neutral clusters." In reality, the smallest nanoparticles include both clusters and large molecules or molecular complexes.

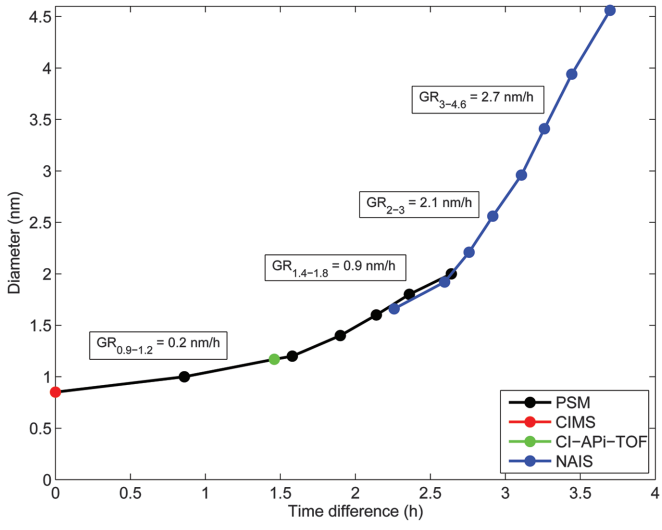

Fig. 2. Cluster size as a function of time during median nucleation event days. Here, we show data from normalized concentrations of sulfuric acid [from a chemical ionization mass spectrometer (CIMS)], size-segregated neutral clusters [from a particle size magnifier (PSM)], a cluster with a mass of 339.06 Th (from CI-APi-TOF), and ions/aerosol particles [neutral cluster and air ion spectrometer (NAIS)]. Times when the concentrations reached half of their maximum are plotted. Because sulfuric acid concentration rises first, the zero time is taken from the value of sulfuric acid. The used mobility diameters of a sulfuric acid molecule and a cluster with a mass of 339.06 Th are 0.85 and 1.17 nm, respectively. Growth rates (GR) for particles below 5-nm diameter were determined using the plotted data. The data with error bars are given in the supplementary materials (section 4 and fig. S15).

Figure 1 shows the median neutral cluster concentrations in different size classes and sulfuric acid concentrations during the nucleation event days (33 days) and nonevent days (19 days). The first thing we observe is the near-constant presence of neutral clusters throughout the sub–2-nm size range (see also fig. S8). This feature indicates continuous formation of neutral clusters and their subsequent growth up to a mobility diameter of at least 2 nm. Concentrations of neutral clusters were typically 10 times higher than concentrations of aerosol particles in the nucleation mode (3- to 12-nm diameter). The second important feature, discussed in more detail below, is the very different behavior of the clusters in three size regimes: (i) <1.2 ± 0.1 nm, (ii) from 1.2 ± 0.1 nm to 1.7 ± 0.2 nm, and (iii) >1.7 ± 0.2 nm. In the first size regime (the size classes 0.9 to 1.1 nm and 1.1 to 1.3 nm in Fig. 1), cluster concentrations and their diurnal behavior were very similar between the nucleation event and nonevent days. In the two other size regimes, cluster concentrations showed a clear daytime maximum during the nucleation event days, which was absent during the nonevent days. The cluster maxima peaked somewhat later than the sulfuric acid concentration. Cluster concentrations decreased rapidly with the increasing cluster size in the first two size regimes. In the third size regime, cluster concentration appeared to increase with the increasing cluster size around noon on nucleation event days (see also fig. S9A). The maximum concentrations of 1.9- to 2.1-nm neutral clusters were about a factor of 50 higher during the nucleation event days compared with the nonevent days.

Several groups have suggested that gaseous sulfuric acid is the main driver of daytime atmospheric aerosol formation (*1*, *10*–*12*). During our measurement campaign, we observed a clear association between the sulfuric acid concentration and the formation rate of 1.5-, 2.0-, and 3.0-nm clusters and aerosol particles (supplementary materials, section 5, and figs. S16 to S18). To look closer at this association, we determined the average growth rates of neutral sub–3-nm clusters during the periods of active aerosol formation (Fig. 2; see also supplementary materials, section 4). These rates were equal to 0.2, 0.9, and 2 nm h^{-1} in the mobility diameter ranges

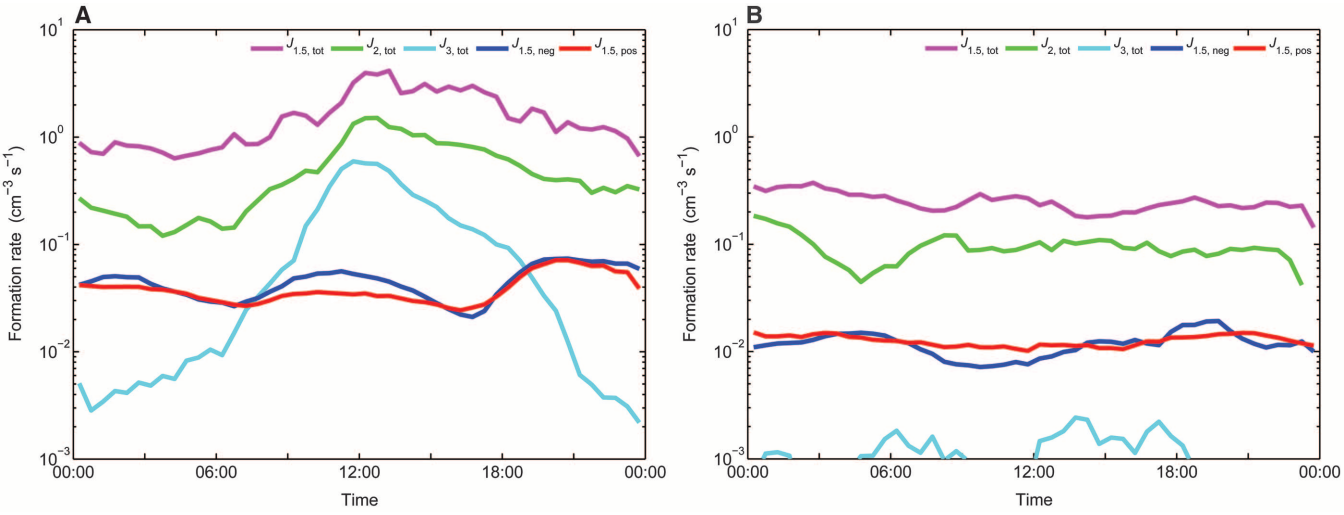

Fig. 3. Average diurnal cycle of the formation rates of 1.5-, 2.0-, and 3.0-nm atmospheric aerosol particles (or clusters) and 1.5-nm negative- and positive-ion clusters during (**A**) nucleation event days and (**B**) nonevent days. The particle-formation rates as a function of sulfuric acid concentration are given in the supplementary materials (section 5 and figs. S16 to S18).

of <1.2, 1.4 to 1.8, and 2 to 3 nm, respectively. An increase in cluster growth rates with increasing particle size in the sub–3-nm size range has recently been reported at two other measurement sites as well (*13*). Next, we calculated the maximum cluster growth rates due to sulfuric acid condensation over the same size ranges by allowing no sulfuric acid evaporation, and we found these rates to be 0.3 to 0.4, 0.6 to 0.9, and 0.5 to 0.6 nm h^{-1}, on average. Clearly, there was more than enough sulfuric acid vapor to explain the growth of the smallest clusters. Together with the very steep decline of cluster concentrations at these sizes, this finding suggests that neutral clusters in the first size regime (<1.2 ± 0.1 nm) both take up and evaporate vapor molecules constantly, the net effect being a slow cluster growth during the periods of active aerosol formation.

In the second size regime (1.2 ± 0.1 to 1.7 ± 0.2 nm), the concentration of sulfuric acid was, within experimental uncertainties, high enough to explain the observed cluster growth rates. On the other hand, quantum chemical investigations (*14*–*17*) predict that clusters containing only sulfuric acid (and water) cannot grow; rather, these clusters must be stabilized with amines, ammonia, or organic vapors (of these, amines are the strongest stabilizers) (*16*). Our measurements obtained by chemical ionization atmospheric pressure interface time-of-flight (CI-APi-TOF) mass spectrometer showed abundant presence of amines in the gas phase, and our APi-TOF measurements showed the existence of sulfuric acid–amine clusters (figs. S5 and S21 to S23). Small sulfuric acid–amine clusters have been identified in earlier laboratory experiments (*18*–*20*) and tentatively also in the atmosphere (*18*).

Clusters in the third size regime (>1.7 ± 0.2 nm) grew two to four times faster than what can be explained by sulfuric acid condensation. Furthermore, the strongest aerosol-formation events were characterized by a local minimum in the size space within this size regime (Fig. 1A and fig. S9A). Such a minimum is in accordance with Nano-Köhler theory (*21*), which describes the activation of neutral clusters by condensable vapors in a manner analogous to cloud condensation nuclei activation by water vapor during cloud formation. After activation, nanoparticles are expected to grow faster due to a decreasing Kelvin effect and, thus, an enhanced condensation flux. The most likely candidates for the additional compounds participating in the growth of sub–3-nm clusters and nanoparticles are organic vapors (*22*–*24*). The cluster activation in the size range of 1.5 to 2.0 nm could be caused by condensation of low-volatility organic vapors once they have overcome the Kelvin barrier (*21*, *25*) or by heterogeneous reactions between the clusters and organic vapors (*24*).

The CI-APi-TOF instrument detects a wide range of molecules and clusters in the 300- to 700-thomson (Th) range, mainly believed to result from highly oxidized organic molecules, similar to those recently found in the ambient APi-TOF measurements by Ehn *et al.* (*26*). The temporal behavior of the ions in this size range is highly variable, with some ions observed mainly at night and others during the day. During periods with high solar radiation, the most abundant cluster above 300 Th is typically detected at 339.06 ± 0.02 Th and has tentatively been identified as $C_{10}H_{15}N_2O_{11}^-$, with one or both N atoms resulting from clustering with nitrate and/or nitric acid inside the CI-APi-TOF instrument. Several other clusters in the 300- to 700-Th range show similar time behavior, and the cluster at 339 Th will be used to represent this group. Although the CI-APi-TOF detection and quantification of organics still needs detailed characterization, our results show that the diurnal variation in the signal of the 339-Th tracks 1.5- to 2.0-nm cluster concentrations even better than sulfuric acid (supplementary materials, section 6, and fig. S20). The total estimated concentration of highly oxidated organic molecules in the 300- to 450-Th range correlated positively with cluster concentrations in the second size regime during active aerosols formation (but not at any other time; see supplementary materials, table S5), indicating that these organic molecules will participate in atmospheric nucleation.

The net flux of growing clusters past a certain size, usually some fixed mobility diameter d, is defined as the formation rate J_d (*8*). Figure 3 shows the formation rates of ions and neutral nanoparticles over the diurnal cycle of an average particle-formation (nucleation) event day and nonevent day. During the nonevent days, the formation rates of 1.5-nm ions averaged to ~0.01 cm^{-3} s^{-1} and showed little diurnal variability. The formation rates of 1.5- and 2.0-nm neutral clusters exceeded 0.1 cm^{-3} s^{-1}, whereas the formation rates of 3-nm particles were mostly too low to be detected. During the days with active aerosol formation, the average formation rates of 1.5-nm ions approached 0.08 cm^{-3} s^{-1} around noon and late evening/early night. The average formation rates of neutral 1.5-nm particles exceeded those of 1.5-nm ions by about one order of magnitude and by up to a factor of 50 to 100 during the afternoon. The formation rates of 3-nm particles were measurable over the whole diurnal cycle of a typical nucleation event day, with values of J_3 approaching J_2 during a few hours around noon. This observation shows the importance of the enhanced growth rate from sub–2-nm size to 3 nm. The formation rate of 3-nm particles during event days was 100 to 1000 times higher than during nonevent days, with the corresponding difference at 1.5 or 2 nm being less than one order of magnitude.

The formation rate of 1.5-nm clusters is often called the atmospheric nucleation rate (*27*). However, from a thermodynamic point of view, nucleation requires overcoming the free energy

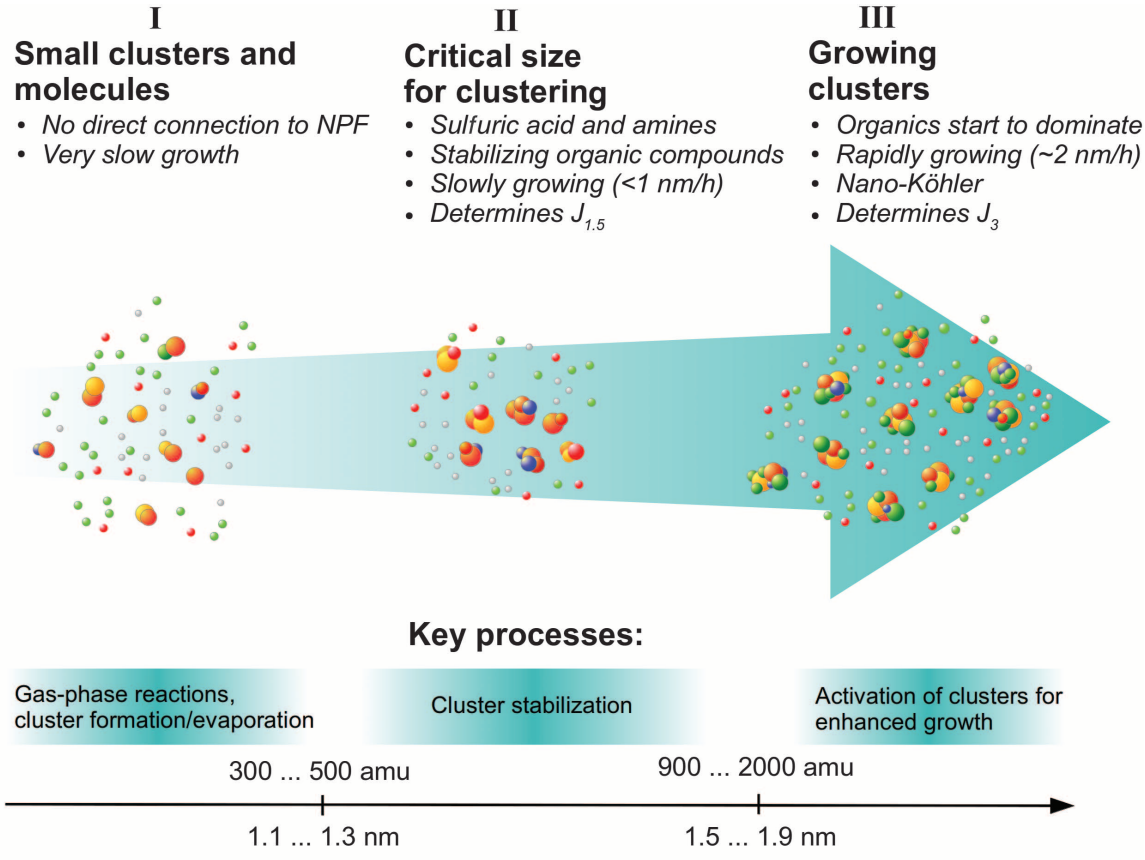

Fig. 4. Schematic description of main size regimes of atmospheric neutral clusters and the main processes related to those size ranges. In regime I (mobility diameter < 1.1 to 1.3 nm), the net cluster growth is very small, as clusters and molecules are continually formed and lost as a result of chemical reactions, vapor uptake, and evaporation. This regime has no direct connection to atmospheric nucleation. NPF, new particle formation. In regime II (1.1 to 1.3 nm to 1.5 to 1.9 nm) clusters grow in size by sulfuric acid condensation and are simultaneously being stabilized by amines, ammonia, or organic vapors. This regime is critical for the clustering process (atmospheric nucleation) and the formation rate of 1.5-nm neutral clusters. Additionally, gas-phase chemical reactions are important in this size range, and activation of clusters will begin. In regime III (>1.5 to 1.9 nm), clusters grow faster than can be explained by sulfuric acid concentration, especially during the periods of active aerosol formation when large numbers of 3-nm aerosol particles are being formed. This fast rate of growth is due to enhanced vapor uptake (most likely of oxidized organic vapors). The key process is activation, by which vapors can contribute to the enhanced growth. In addition, clustering plays a role, and condensable vapors are produced via chemical reactions. amu, atomic mass units.

barrier. The relatively high evaporation flux in the first size regime indicates the existence of a nucleation barrier and that the critical cluster in the atmospheric nucleation point of view is in the second size regime at 1.5 ± 0.3 nm. In any case, we observe a starting point of a phase transition, which includes chemical reactions to form condensable vapors, heteromolecular clustering of vapor molecules, and the subsequent growth of clusters to 2 and 3 nm.

In summary, we can identify three separate size regimes characterized by different mobility diameter ranges for neutral clusters (Fig. 4). Our findings demonstrate an observational-based framework on atmospheric aerosol formation that, in a consistent way, combines (i) molecules, small atmospheric clusters, and growing nanoparticles; (ii) sulfuric acid, strong bases, and organic vapors; and (iii) various dynamical processes. This framework confirms that atmospheric aerosol formation is essentially a two-step process, as suggested based on theoretical arguments (*21*, *28*) and some laboratory experiments (*29*). In the first step—in the second size regime—atmospheric nucleation or the formation of stabilized clusters will occur. The second step, characterized by enhanced cluster growth rates due to the activation of the growing clusters by organic vapors, is initiated in the third size regime just below 2 nm. This second step determines the formation rate of 3-nm particles and is efficient only during periods of active aerosol formation. Our findings emphasize the important role of organic compounds in atmospheric aerosol formation; in the radiative forcing that results when these particles grow to larger sizes; and in the associated feedbacks involving the biosphere, clouds, and climate (*30*, *31*).

References and Notes

1. M. Kulmala *et al.*, *J. Aerosol Sci.* **35**, 143 (2004).
2. R. Zhang, A. Khalizov, L. Wang, M. Hu, W. Xu, *Chem. Rev.* **112**, 1957 (2012).
3. D. V. Spracklen *et al.*, *Atmos. Chem. Phys.* **6**, 5631 (2006).
4. J. Merikanto, D. V. Spracklen, G. W. Mann, S. J. Pickering, K. S. Carslaw, *Atmos. Chem. Phys.* **9**, 8601 (2009).
5. J. Kazil *et al.*, *Atmos. Chem. Phys.* **10**, 10733 (2010).
6. R. Makkonen *et al.*, *Atmos. Chem. Phys.* **12**, 1515 (2012).
7. P. Hari, M. Kulmala, *Boreal Env. Res.* **10**, 315 (2005).
8. M. Dal Maso *et al.*, *Boreal Env. Res.* **10**, 323 (2005).
9. A. Hirsikko *et al.*, *Atmos. Chem. Phys.* **11**, 767 (2011).
10. R. Weber *et al.*, *Chem. Eng. Commun.* **151**, 53 (1996).
11. V.-M. Kerminen *et al.*, *Atmos. Chem. Phys.* **10**, 10829 (2010).
12. M. Sipilä *et al.*, *Science* **327**, 1243 (2010).
13. C. Kuang *et al.*, *Atmos. Chem. Phys.* **12**, 3573 (2012).
14. T. Kurtén, V. Loukonen, H. Vehkamäki, M. Kulmala, *Atmos. Chem. Phys.* **8**, 4095 (2008).
15. V. Loukonen *et al.*, *Atmos. Chem. Phys.* **10**, 4961 (2010).
16. I. K. Ortega *et al.*, *Atmos. Chem. Phys.* **12**, 225 (2012).
17. P. Paasonen *et al.*, *Atmos. Chem. Phys.* **12**, 9113 (2012).
18. J. Zhao *et al.*, *Atmos. Chem. Phys.* **11**, 10823 (2011).
19. T. Petäjä *et al.*, *Phys. Rev. Lett.* **106**, 228302 (2011).
20. B. R. Bzdek, D. P. Ridge, M. V. Johnston, *Atmos. Chem. Phys.* **11**, 8735 (2011).
21. M. Kulmala, V.-M. Kerminen, T. Anttila, A. Laaksonen, C. D. O'Dowd, *J. Geophys. Res.* **109**, D04205 (2004).
22. A. Metzger *et al.*, *Proc. Natl. Acad. Sci. U.S.A.* **107**, 6646 (2010).
23. P. Paasonen *et al.*, *Atmos. Chem. Phys.* **10**, 11223 (2010).
24. L. Wang *et al.*, *Nat. Geosci.* **3**, 238 (2010).
25. N. M. Donahue, E. R. Trump, J. R. Pierce, I. Riipinen, *Geophys. Res. Lett.* **38**, L16801 (2011).
26. M. Ehn *et al.*, *Atmos. Chem. Phys.* **12**, 5113 (2012).
27. M. Kulmala *et al.*, *Science* **318**, 89 (2007).
28. M. Kulmala, L. Pirjola, J. M. Mäkelä, *Nature* **404**, 66 (2000).
29. P. E. Wagner, R. Strey, *J. Phys. Chem. B* **105**, 11656 (2001).
30. M. Kulmala *et al.*, *Atmos. Chem. Phys.* **4**, 557 (2004).
31. K. Carslaw *et al.*, *Atmos. Chem. Phys.* **10**, 1701 (2010).

Acknowledgments: This work was funded by the European Research Council Project (grant nos. 227463-ATMNUCLE and 257360-MOCAPAF). We thank the Academy of Finland Centre of Excellence program and related projects (grants nos. 1118615 and 1127372) for support.

Supplementary Materials

www.sciencemag.org/cgi/content/full/339/6122/943/DC1
Materials and Methods
Supplementary Text
Figs. S1 to S24
Tables S1 to S7
References (*32*–*65*)

12 July 2012; accepted 12 December 2012
10.1126/science.1227385